Applied Surface Science 741 (2026) 167074

Contents lists available at ScienceDirect

Applied Surface Science

journal homepage: www.elsevier.com/locate/apsusc

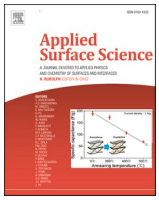

Full Length Article

Ultrafast and reversible adsorption of methylene blue on covalently sulfonated reduced graphene oxide

Ludovica Ceroni [a,b], Samuel Pressi [a,b], Laura Calvillo [a,b], Ester Marotta [a,b], Enzo Menna [a,b,c,*]

[a] Dipartimento di Scienze Chimiche, Università di Padova, Via Marzolo 1, 35131 Padova, Italy
[b] Consorzio Interuniversitario Nazionale per la Scienza e Tecnologia dei Materiali (INSTM), Via G. Giusti, 9, 50121 Firenze, Italy
[c] Istituto per la Tecnologia delle Membrane del CNR "Enrico Drioli", Sede Secondaria di Padova, Via Marzolo, 1, 35131 Padova, Italy

ARTICLE INFO

Keywords:
Graphene
Functionalization
Adsorption
Dye
Water treatment

ABSTRACT

Carbon-based nanomaterials are widely studied for water purification owing to their high surface area and tunable surface chemistry. Among them, graphene derivatives often outperform activated carbon and carbon nanotubes, though their application is limited by aggregation and poor dispersibility. Here, we report the synthesis of sulfonated reduced graphene oxide (rGO-S) via diazotization with sodium sulfanilate. Covalent grafting of benzenesulfonate groups was confirmed by TEM, EDX, XPS, FTIR, and TGA, showing homogeneous functionalization and improved dispersibility (0.49 mg/mL). The highly negative zeta potential (−45.3 mV) prevents aggregation and enhances accessible adsorption sites.

The covalently sulfonated graphene exhibited ultrafast adsorption kinetics for methylene blue, reaching equilibrium within less than one minute, which is considerably faster than previously reported graphene-based adsorbents.

Kinetics followed a pseudo-second-order model, with an adsorption capacity of 326 mg/g – twice that of pristine rGO. The material also demonstrated efficient regeneration through ion exchange with NaCl (combined with ethanol), achieving up to 92% desorption over multiple cycles while maintaining stable performance. Selectivity tests in dye mixtures confirmed preferential methylene blue uptake driven by electrostatic interactions with sulfonate groups.

Overall, rGO-S combines ultrafast kinetics, high efficiency, selectivity, and reusability, highlighting its potential for water treatment and pollutant recovery applications.

1. Introduction

In the field of water and wastewater treatment, significant scientific research is focusing on nanomaterial-based adsorbents due to their powerful capacities to remove a large range of organic pollutants [1–3]. Specifically, in recent times there has been a notable evolution in the study of carbon-based nanomaterials for environmental purification [4–6]. The nanometric size and large surface area of nano-adsorbent indeed provides numerous active adsorbing sites, resulting in the effective interaction with different chemical species. Moreover, carbon nanostructures exhibit tunable surface reactivity, thermal and chemical stability, vast availability, and catalytic potential at the nanoscale [7].

Graphene and its derivatives have been identified as particularly effective nano-adsorbents for the treatment of polluted water [8,9]. The adsorption mechanisms mainly include π–π and n–π interactions, hydrophobic interactions, hydrogen bonding and electrostatic interactions depending on the specific pollutant [10]. The superior adsorption capacity of graphene is attributable to its extensive specific surface area, up to 2630 m^2/g, thereby generating a higher number of binding sites respect to other adsorbents [11].

Compared to carbon nanotubes (CNT), the opened-up layer structure of graphene results in significantly faster adsorption kinetics and adsorption capacity [12]. On the other hand, activated carbon (AC), which represents the benchmark for adsorption processes, demonstrated lower efficiency compared with graphene derivatives [13]. Moreover, the implementation of AC is constrained by its unfavorable kinetics, limited regeneration capability and the absence of selectivity of its active sites towards specific pollutants [14].

It should be noted, however, that the use of graphene as adsorbent also exhibits some limitations due to its inert and hydrophobic nature.

* Corresponding author at: Dipartimento di Scienze Chimiche, Università di Padova, Via Marzolo 1, 35131 Padova, Italy.
E-mail address: enzo.menna@unipd.it (E. Menna).

https://doi.org/10.1016/j.apsusc.2026.167074
Received 13 February 2026; Received in revised form 21 April 2026; Accepted 29 April 2026
Available online 2 May 2026

This results in the reaggregation of graphene sheets, thus reducing the effective surface area and the accessibility of sorption sites, thereby dramatically limiting the adsorption efficiency of these materials [15].

These drawbacks may be overcome by functionalization with polar or charged functional groups. The functionalities can increase the wettability of graphene sheets and repel them from each other, thereby facilitating the formation of individual nanostructures in homogeneous dispersions [8,16]. Consequently, surface modification makes new active sites available for the interaction with pollutants by enhancing the specific surface area. In addition, graphene can be functionalized with suitable functional groups, which can interact specifically with polar or charged organic compounds through hydrogen bonding or electrostatic interactions. This approach enhances the adsorption performances of the materials.

Most studies are based on graphene oxide (GO) which exhibits oxygen-containing surface functionalities and highly hydrophilic properties that improve the adsorption process. Specifically, the oxygen-containing groups (i.e. carboxyl, hydroxyl, carbonyl and epoxy) formed upon harsh oxidation of graphite allow for a high negative charge density, which consequently enables good water dispersibility and binding of positively charged organic molecules via electrostatic interactions and coordination [17].

Also used in the present study, methylene blue (MB) is widely employed as a positively charged model pollutant. Specifically, MB is a thiazine basic dye used in various industries, including textiles, printing, paints, pharmaceuticals, medicine and food [18–20]. Despite not being highly toxic, it causes significant environmental damage [18] and poses risks to human health [21].

In the case of MB, GO showed extraordinary adsorption capacity and fast adsorption rates [13,22–24]. Nevertheless, the required treatments with strong oxidants or oxidizing acids lead to uncontrolled and inhomogeneous surface functionalization [17], limiting the reproducibility of the synthesis and inducing variability in the adsorption performance. Moreover, GO is characterized by holes and structural defects that decrease the surface area available for adsorption, thus hampering the interaction with pollutants.

A more extended sp^2 carbon surface, available for hydrophobic and π-π interactions with pollutants, is offered by reduced GO (rGO), which has usually a lower cost and better processability than pristine graphene. Indeed, it has been shown that adsorption of organic chemicals with large molecular size and extended aromatic structures occurs with faster kinetic and larger capacity on rGO compared to GO [25,26]. On the other hand, reduction of GO to rGO can result in the almost complete loss of oxygen moieties, with poor control over the residual groups, which decreases the dispersibility in water.

The reactivity of oxygenated groups present on GO or rGO surface, including carboxyl groups, hydroxyl groups, or epoxides, can be used for a further chemical modification of the nanostructures, through amidation, esterification or epoxide ring-opening reactions [27,28].

Despite the large number of graphene-based adsorbents reported for dye removal, several limitations remain, including slow adsorption kinetics, aggregation of graphene sheets in aqueous media, and limited reusability of the adsorbent.

In particular, many graphene derivatives reported in the literature are obtained through hydrothermal or oxidative routes, which may result in heterogeneous functionalization and limited control of surface chemistry. Covalent functionalization strategies that provide stable and well-defined surface groups while preserving the high accessibility of graphene surfaces remain relatively less explored for adsorption applications.

A simple, fast and potentially scalable alternative functionalization method is the diazotization reaction, first proposed by Tour et al. [29], based on aryl diazonium chemistry. Starting from an aniline precursor, the Tour reaction results in the covalent attachment of substituted benzene rings on the graphene basal plane without massive damage [30,31]. The reaction allows the preparation of tailored functional materials with improved dispersion capability in organic solvents such as DMF [32] and in water [33], by simply changing the substituents of the aniline reagent [34,35]. The presence of substituted benzene rings prevents π-π stacking induced aggregation through steric repulsion between the decorated surfaces and improved interaction with the solvent.

In this context, the covalent grafting of sulfonated aromatic groups through diazonium chemistry represents a promising approach to tailor the surface charge and dispersibility of graphene materials. Such functionalization can enhance electrostatic interactions with cationic pollutants while preventing aggregation of graphene sheets in aqueous media, thereby improving adsorption efficiency and kinetics. Indeed, according to this strategy, we previously synthesized multi-walled CNT derivatives bearing benzenesulfonate groups (MWCNT-S) [36,37] with remarkable water solubility and MB adsorption efficiency. Moreover, the adsorption mechanism of MWCNT-S, involving electrostatic interactions, enabled desorption of pollutants through an ion exchange process [36].

In the present work, rGO was covalently functionalized with benzenesulfonate groups following the same approach. Unlike previously reported sulfonated graphene materials, obtained for example through hydrothermal sulfonation [38], or through diazotization of GO followed by reduction [39–41], or similar approaches also involving carboxylic groups of GO [42], the present work employs an optimized diazonium covalent functionalization of rGO which provides improved colloidal stability.

The resulting material (rGO-S) exhibits excellent aqueous dispersibility, high surface charge, and extremely fast adsorption kinetics for methylene blue removal from water. In addition, efficient regeneration of the adsorbent and selective adsorption behavior in dye mixtures are demonstrated, highlighting the potential of this material for practical water purification applications.

In the present study, MB is employed as a positively charged model pollutant. Specifically, MB is a thiazine basic dye used in various industries, including textiles, printing, paints, pharmaceuticals, medicine and food [18–20]. Despite not being highly toxic, it causes significant environmental damage [18] and poses risks to human health [21]. Thanks to its sp^2 extended structure, water solubility and facility to identify in water, MB is widely employed for testing and comparing adsorption properties of adsorbents.

Adsorption of MB by rGO-S has been studied in terms of kinetics, capacity and mechanism and has been compared with pristine rGO and with previous studies in the relevant literature.

Previous studies reporting sulfonated graphene adsorbents, besides being based on different synthetic procedures, focus primarily on adsorption capacity, while less attention has been devoted to adsorption kinetics, dispersibility, and regeneration, which are crucial for practical water treatment applications.

The main novelty of the present work lies in the covalent functionalization of reduced graphene oxide with benzenesulfonate groups through optimized diazonium chemistry, which provides highly dispersible graphene sheets with a strong negative surface charge.

2. Materials and methods

Graphene material (rGO) with flake diameter in the range 0.4–5 μm, thickness in the range 0.6–1.2 nm and BET surface area of 400 ~ 1000 m^2/g was purchased from ACS Material (Pasadena, CA, USA). All other reagents and solvents were purchased from Sigma-Aldrich (Milan, Italy) and used as received if not otherwise specified.

2.1. General procedures

The equipment used and the common procedures followed for sample treatments are described hereafter.

2.1.1. Bath sonication

Sonication for sample dispersion was carried out with an ultrasonic bath Sonorex Super RK 100H (Bandelin Electronic GmbH & Co. KG, Berlin, Germany), operating at 112 W.

2.1.2. Tip sonication

Pulsed microtip sonication was carried out for 1 min using a Misonix S-3000 sonicator (Misonix Incorporated, Farmingdale, NY, USA) equipped with a titanium tip (power level: 2.0, 4–6 W; pulse on: 3 s; pulse off: 3 s).

2.1.3. Preparation of solutions for the adsorption experiments

Each solution for the adsorption experiments was prepared by first dispersing the adsorbent in water through bath sonication (5 min) and then adding a proper dye solution to reach the final desired concentration of adsorbent and pollutant in a volume of 25 mL.

2.1.4. Shaking during adsorption and desorption experiments

The flasks containing the adsorbent and the pollutant solutions were kept in a shaker incubator VWR Professional 3500 (VWR International S. r.l, Milan, Italy) at 150 rpm and 25 °C.

2.1.5. Centrifugation

Centrifugation of the samples was carried out with a Thermo Scientific MR23i Centrifuge (Thermo Electron LED GmbH, Osterode, Germany).

2.1.6. Preparation of solutions for the UV analysis

Prior to UV analysis, each solution was filtered to separate the adsorbent from the solution. This process was carried out using disposable J.T. Baker syringe filters (VWR International S.r.l, Milan, Italy), PES, 0.1 μm, 30 mm, discarding the first 20 mL and keeping the last 4 mL for the analysis.

2.2. Synthesis of rGO-$PhSO_3^-$ (rGO-S)

rGO (52.0 mg, 4.33 mmol of carbon) and sodium sulfanilate dihydrate (500.5 mg, 2.16 mmol, 0.5 eq relative to carbon) were added in a flask with 7.5 mL of Milli-Q water and the mixture was degassed with N_2 for 15 min. The reaction mixture was heated to 80 °C under N_2 flux and magnetic stirring; then isopentyl nitrite (0.612 mL, 95%, 4.33 mmol, 1 eq relative to carbon) was added. After 4 h the reaction mixture was cooled to room temperature. The dispersion was filtered on a Millipore PC 0.1 μm membrane (VCTP) and the product was washed on the filter with 50 mL of distilled water and then removed from the filter through sonication in 50 mL of distilled water. The filtration/washing procedure was repeated five times using water:methanol (1:1) and one time using methanol. The functionalized product with benzenesulfonate groups, rGO-$PhSO_3^-$ (rGO-S), was finally removed from the filter by bath sonication in methanol and dried under N_2 flux.

2.3. Characterization of rGO-S

2.3.1. Transmission electron microscopy (TEM)

The morphology and microstructure of the samples were characterized by TEM and high-angle annular dark-field (HAADF) scanning transmission electron microscopy (HAADF-STEM) using TEM JEOL F200 operated at 200 kV. Elemental analysis and mapping were performed using a JEOL 100 mm^2 silicon drift energy dispersive X-ray spectrometer (EDX). For the sample preparation, 1 mg of nanostructure was dispersed in 1 mL of ethanol by tip sonication. One drop of the dispersion (about 25 μL) was placed on a carbon supported copper grid, 400 mesh size.

2.3.2. X-ray photoelectron spectroscopy (XPS)

XPS spectra were registered with an Omicron EA125 electron analyser and an Omicron DAR 400 X-ray source with a dual Al − Mg anode in a custom-made ultra-high vacuum system working at 10^{-10} mbar. Core-level photoemission spectra (C 1s, N 1s, S 2p, O 1s regions) were collected with a non-monochromatized Al Kα X-ray source (1486.3 eV) in normal emission at room temperature. Measurement parameters were set at 0.1 eV steps, 0.5 s collection time, and 20 eV pass energy.

2.3.3. Thermogravimetric analysis (TGA)

Thermogravimetric analysis was performed on powdered samples using a TGA Q5000IR instrument (TA instruments, New Castle, DE, USA) and a 100 μL Platinum HT TAG pan. The measurement method included an isotherm at 100 °C for 10 min to remove possible traces of residual solvents followed by a ramp at 10 °C/min up to 1000 °C in N_2 atmosphere. The thermograms were processed by TA TRIOS software.

2.3.4. Preparation of rGO-S standard dispersion

rGO-S (5 mg) was dispersed in 2.5 mL of Milli-Q water by tip sonication for 1 min. The dispersion was centrifuged at 2000 rpm for 10 min to precipitate the less dispersible fraction. The supernatant was recovered and filtered over cotton wool to remove fluffy, large and lightweight aggregates potentially non-precipitated during the centrifugation process and results in a filtrate which is the rGO-S standard dispersion.

2.3.5. Measurement of dispersibility

The dispersibility in water of the rGO-S derivative is defined as the concentration (m/V) of a standard dispersion obtained through the above-described procedure. The concentration was measured through the following procedure. A known volume (1 mL) of standard dispersion was drop cast on a calibrated pan and a TGA measurement consisting of an isotherm at 100 °C for 15 min in air provided the dry weight used to calculate the m/V concentration.

2.3.6. Dynamic Light Scattering (DLS) and Zeta Potential (ZP)

100 μL of the rGO-S standard dispersion was added to 1.0 mL of Milli-Q water in a disposable plastic cuvette with an optical path of 1 cm for DLS analysis. The DLS measurement was performed using a Zetasizer Nano S analyzer (Malvern Instruments, Malvern, UK) setting the measurement angle at 173°, backscatter (NIBS default), water as solvent, temperature at 25 °C and equilibration time at 120 s. The reported value is an average of 3 measurements of 11 runs each, with a run duration of 10 s.

100 μL of the rGO-S standard dispersion was added to 700 μL of Milli-Q water and to 160 μL of a solution 1 mg/mL of NaCl in water in a folded capillary cell for Zeta Potential analysis. ZP measurement was carried out equilibrating at 25 °C for 120 s. The Smoluchowski equation was used as theoretical model for the measurement, and the resulting value is an average of 3 measurements of 10–100 runs each.

2.4. Preparation of pollutant solutions

A stock solution 250 mg/L of methylene blue (MB) was prepared by dissolving 62.5 mg in 250 mL of Milli-Q water. Solutions for adsorption experiments (excluding the selectivity study; see section 2.6.5) were prepared by diluting the stock solutions with milliQ water to the desired concentration.

2.5. Analysis and quantification of pollutants

Analyses of MB were performed by using a Varian Cary 100 spectrophotometer (Agilent Technologies, Santa Clara, CA, USA), between 280 nm and 1400 nm at room temperature. The quantification of MB was performed through an external calibration method by recording the absorbance of solutions with different pollutant concentrations and by analyzing the peak at 665 nm. The linearity was investigated in the range between 0.5–4 mg/L.

Analyses of mixture of dyes (MB; methyl orange (MO); rhodamine B (RhB)) were performed using an HPLC-UV (Agilent Technologies 1260 Infinity II) with a variable wavelength UV detector (VWD) acquiring the signal at 254 nm. The chromatographic separation was performed using a Kinetex 5 μm C18 100 Å, 150 x 4.6 mm column (Phenomenex). The eluents used were acetonitrile (B) and Milli-Q water (A), both acidified to 0.1% V/V with formic acid. The gradient for eluent B was as follows: 10% for 1 min, from 10% to 100% in 25 min, isocratic at 100% for 2 min. The flow rate was set at 1 mL/min, and the injection volume was 10 μL. The quantification of dyes was performed through external calibration by integrating the area of the chromatographic peaks at 9.2, 10.2 and 14.5 min for MB, MO and RhB solutions respectively with different pollutant concentrations. The linearity was assessed in the range between 1–5 mg/L.

2.6. Adsorption experiments

2.6.1. Batch kinetic experiments

The adsorption experiments to determine the effect of the contact time on the amount of dye adsorbed were performed treating 5 mg of adsorbent (either rGO or rGO-S) with 25 mL of MB solution with a concentration of 50 mg/L for a variable adsorption time from 1 to 180 min. The percentage of MB in solution after adsorption was calculated according to equation (1).

$$\text{Residual MB}\,(\%) = \frac{C_t}{C_0}\cdot 100 \tag{1}$$

where C_0 (mg/L) is the initial concentration of MB and C_t (mg/L) is the residual concentration of MB in solution after the adsorption time t.

The data analysis was performed by fitting the experimental data with the pseudo-first-order and the pseudo-second-order kinetic models, using eqs. (2) and (3), respectively [43].

$$\log\,(q_{eq}\text{-}q_t\,) = \log(q_{eq})\text{-}\frac{k_1}{2.303}\,t \tag{2}$$

$$\frac{t}{q_t} = \frac{1}{k_2 q_{eq}^2} + \frac{t}{q_{eq}} \tag{3}$$

where q_{eq} (mg/g) is the equilibrium adsorption capacity, q_t (mg/g) is the adsorption capacity of the material at time t, k_1 (1/min) is the pseudo-first-order equilibrium rate constant and k_2 (g/(mg·min)) is the pseudo-second-order equilibrium rate constant.

2.6.2. Batch equilibrium experiments

To determine the effect of the initial dye concentration on adsorption, a series of adsorption experiments were carried out treating 5 mg of adsorbent (either rGO or rGO-S) with 25 mL of MB solutions for 1 h. The MB concentrations were 40, 50, 70, 80, 100 and 120 mg/L for rGO and 50, 70, 80, 100, 120 and 150 mg/L for rGO-S. The adsorption capacity (mg/g) at equilibrium was calculated using eq. (4).

$$q_{eq} = \frac{(C_0 - C_{eq}) \bullet V}{m} \tag{4}$$

where C_{eq} (mg/L) is the equilibrium concentration of MB in solution after 1 h, V (L) is the volume of the solution and m (g) is the mass of the adsorbent.

The data analysis was performed by fitting the experimental data with Langmuir and Freundlich isotherm models using eqs. (5) and (6), respectively [44].

$$\frac{C_{eq}}{q_{eq}} = \frac{C_{eq}}{q_m} + \frac{1}{K_L q_m} \tag{5}$$

$$\log\left(q_{eq}\right) = \log(K_F) + \frac{1}{n}\log(C_{eq}) \tag{6}$$

where q_m (mg/g) is the maximum adsorption capacity of the material, K_L (L/mg) is the Langmuir constant, instead, K_F and 1/n are Freundlich constants that represent, respectively, the adsorption capacity and the intensity of adsorption.

Batch kinetic and batch isotherm tests were repeated in triplicate to ensure statistical significance of the measurements. The reported values are the average obtained from the three experiments, with the corresponding standard deviation calculated using eq. (7).

$$\sigma = \sqrt{\frac{\sum_{i=1}^{3}(q_{eq,i} - \overline{q_{eq}})^2}{2}} \tag{7}$$

2.6.3. Desorption tests

The desorption tests were carried out on rGO-S previously subjected to MB adsorption under equilibrium conditions, using 5 mg of adsorbent into 25 mL of MB solution with a concentration of 100 mg/L for 1 h. After adsorption, the saturated rGO-S was recovered through centrifugation (at 5000 rpm for 20 min), and the MB concentration in the supernatant was determined from UV–Vis absorbance. The adsorbent was subsequently washed with 20 mL of Milli-Q water in order to remove any residual MB (not adsorbed) and was then recovered through centrifugation. Different desorption conditions were tested by dispersing saturated rGO-S samples in the desorption solvents (or solutions), keeping the flask in an ultrasonic bath for 5 min and then in a shaker incubator for a variable time. The desorption conditions tested are briefly summarized as follows:

D01. 25 mL of EtOH for 1 h.
D02. 25 mL of EtOH for 24 h.
D03. 25 mL of 0.5 M aqueous NaCl for 1 h.
D04. 25 mL of 1 M aqueous NaCl for 1 h.
D05. 40 mL of 1 M aqueous NaCl for 1 h.
D06. 25 mL of 1 M aqueous NaCl for 24 h.
D07. 25 mL of 2 M aqueous NaCl for 1 h.
D08. 25 mL of saturated aqueous NaCl for 1 h.
D09. 25 mL of Milli-Q water for 1 h.
D10. 20 mL of 1 M aqueous NaCl for 1 h, followed by treatment with 20 mL of 1 M aqueous NaCl for 1 h.
D11. 40 mL of 1 M aqueous NaCl for 1 h, followed by treatment with 40 mL of 1 M aqueous NaCl for 1 h.
D12. 40 mL of EtOH for 1 h, followed by treatment with 40 mL of 1 M aqueous NaCl for 1 h and then treatment with 40 mL of 1 M aqueous NaCl for 1 h.

The adsorbent was separated from the solution through centrifugation (at 5000 rpm for 20 min), and the MB concentration in the supernatant was determined by UV–Vis absorbance measurement after each desorption step. The percentage of desorbed dye was calculated with respect to the amount of dye adsorbed on the nanostructure.

2.6.4. Regeneration cycles

The adsorption/desorption cycles were performed on rGO-S samples as described in the previous section, applying the desorption condition D12 and repeating the regeneration cycle three times. After each adsorption/desorption cycle, the adsorbent was washed three times with 40 mL of Milli-Q water to remove residual NaCl and dried in an oven at 60 °C overnight. The dry adsorbent was then weighed and used for the subsequent cycle. The adsorption capacity of rGO-S (mg/g) at equilibrium was calculated using equation (4). The percentage of desorbed dye was calculated with respect to the amount of dye adsorbed on the nanostructure.

2.6.5. Selectivity experiment

For the selectivity experiments, three stock solutions of 50 mg/L of MB, MO and RhB were prepared by dissolving 5 mg of each dye in 100 mL of tap water. The three solutions were then combined and diluted with tap water to obtain a mixture of the three dyes, each at a

concentration of 5 mg/L. The study was carried out by treating 5 mg of adsorbent (either rGO or rGO-S) with 25 mL of the mixture for 1 h. The selectivity was reported as the removal percentage of pollutants with respect to their initial concentration for the different nanostructures.

3. Results and discussion

3.1. rGO-S synthesis and characterization

The surface of commercially available rGO was decorated with benzene sulfonate groups through a diazotization reaction to afford derivative rGO-S, Fig. 1 (details in section 2.2). The diazonium precursor sodium sulfanilate was activated in situ with isopentyl nitrite, following a synthetic strategy readapted from our previous works [36,37,45] and based on the Tour reaction [46]. Briefly, the functionalization was carried out in water at 80 °C, with an amount of aniline and nitrite of 0.5 eq and 1 eq, respectively, relative to graphene carbon moles.

This reaction allows relative control [45], does not require hazardous reagents or toxic contaminants and, being carried in an aqueous environment, it does not leave residues of organic solvents adsorbed on the nanostructures. These characteristics are favorable for application of the resulting materials in water treatment. Indeed, CNT derivatives obtained with the same approach showed good biocompatibility both in vitro and in vivo [37].

TEM images in Fig. 2 show the typical structure of graphene flakes of different sizes. The presence of individual-like flakes is more evident in the rGO-S sample than in pristine rGO where mainly large multilayer aggregates of graphene sheets are visible. This evidence agrees with the better dispersibility of rGO-S, since the samples were deposited on TEM grids from a dispersion in ethanol. Moreover, comparing the two samples no signs of degradation are found in rGO-S, thus confirming that our functionalization mostly preserves basal plane integrity. This observation can also be deduced from the Raman spectra of rGO and rGO-S (**Fig. S1**).

STEM-EDX was employed for the elemental analysis and mapping of a selected area of rGO and rGO-S samples. Comparing the EDX spectra of the two materials (reported in Fig. 3**a and b** respectively), a significant increase in the sulfur signal was observed in rGO-S and the additional sodium counterion signal was detected. Specifically, the calculated atomic percentage of sulfur is 1.69% in rGO-S, which is four times higher than in pristine rGO (where small amounts of S are expected as residues from the production processes) [47]. Fig. 3**c** shows the elemental map of rGO-S, indicating the distribution of elements within the selected area. Besides the presence of C and O signals, which are characteristic of the rGO structure, it is interesting to note that the S and Na signals are uniformly distributed and perfectly follow the sample area. The concentration of the elements also depends on the thickness of the sample. For example, the C, O, S and Na signals are more pronounced where the graphene sheets are folded. These results suggest that the chosen functionalization method decorates both the edges and the basal plane of rGO with benzenesulfonate groups, resulting in a homogeneously functionalized surface.

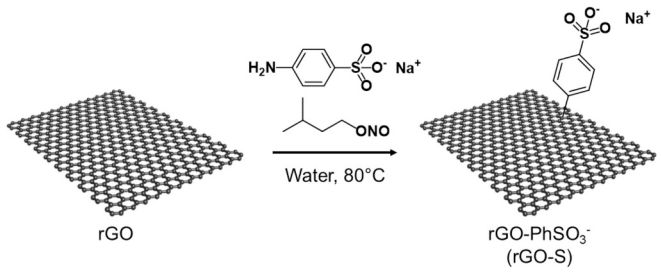

Fig. 1. Schematic representation of the functionalization of rGO with benzenesulfonate groups through diazotization reaction.

The C 1s and S 2p XPS regions of both pristine rGO and functionalized rGO-S were analyzed and reported in Fig. 4**a,b**, while the XPS spectrum of the N 1s region is reported in the supporting information (**Fig. S2**). The deconvolution of the C 1s signal reveals a main peak at 284.1 eV attributed to C sp^2 typical of graphitic materials. Other minor components are detectable at 285.1 eV related to C sp^3, and at 286.2, 287.6 and 288.6 eV ascribed to alcohol, carbonyl and carboxylic groups, respectively; the detailed analysis is reported in Table 1 [48,49]. These results give evidence of the presence of oxygen groups characteristic of rGO. In addition, the rGO-S sample showed an intense peak in the S 2p region at 167.8 eV corresponding to the SO_3^- group, also visible in the spectrum of sodium sulfanilate (Aniline-S), confirming the hypothesis of covalent functionalization with benzenesulfonate groups [50]. Another minor component in the S 2p region is more difficult to interpret and could be attributed to doping of the graphene surface with sulfur atoms. The relative abundance of the two components is reported in Table 2.

The surface composition of rGO-S was obtained from the S 2p, C 1s and O 1s peak regions, with the corresponding sensitivity factors taken into account. As shown in Table 1, the functionalization process introduced 5.2 at.% of sulphur onto the surface. At the same time, the amount of oxygen increased from 4.4 at.% to 16.0 at.%. A comparison with the atomic composition provided by EDX is not possible because the two analyses involve different portions of the samples: indeed, XPS results refer to the most superficial layer.

The chemical composition of rGO and rGO-S was further investigated by means of infrared spectroscopy (**Fig. S3**). This method revealed the presence of the SO_3 stretching vibration mode, thus confirming the nature of the functional groups.

The overlay of the thermograms from TGA analysis of rGO and rGO-S is shown in **Fig. S4**. Specifically, rGO-S derivative exhibits a weight loss of 12.7% between 100–600 °C relative to the pristine nanostructure, consistent with thermal degradation of organic groups. Based on this analysis, the functionalization degree (FD), defined as the ratio between the number of moles of the functional group and the total moles of remaining carbon, can be calculated (details on FD calculation are described in the Supporting Info, **S5**), affording a value of 2.46%. It is worth mentioning that FD calculation includes C atoms of all graphene layers, including the inner ones, that are not involved in the functionalization.

To evaluate the effectiveness of functionalization in promoting disaggregation of the nanostructures, as reported in our previous works [36,51], a standard water dispersion of rGO-S was prepared through the procedure described in section 2.3.4. Water dispersibility resulted in 0.49 mg/mL and DLS analysis afforded a hydrodynamic mean diameter of 655 ± 23 nm for the rGO-S particles in water. This result is in agreement with other graphene water dispersions documented in the literature [52–54]. Graphene nanostructures, in fact, have strong tendency for agglomeration and precipitation in solution even with a high degree of functionalization. On the other hand, pristine rGO is fully insoluble in water, which even precludes the possibility of performing DLS analysis. The PdI of the rGO dispersion was 0.297, corresponding to a moderately polydisperse size distribution. A high negative Zeta potential value of −45.3 ± 1.0 mV was found, consistent with the negative charges of the sulfonate groups [55]. Overall, such observations confirm that the charged sulfonate units prevent the graphitic sheets from aggregating in solution, thereby yielding isolated sheets of rGO-S with improved water solubility.

3.2. Adsorption experiments

3.2.1. Kinetics adsorption studies

The adsorption kinetics were studied for rGO and rGO-S to assess the time required by the adsorbents to reach equilibrium with the contaminant in solution. The tests were carried out treating the adsorbent with a solution of MB at variable contact times and results are reported in Fig. 5**a** as residual percentage of MB after adsorption. It is already clear

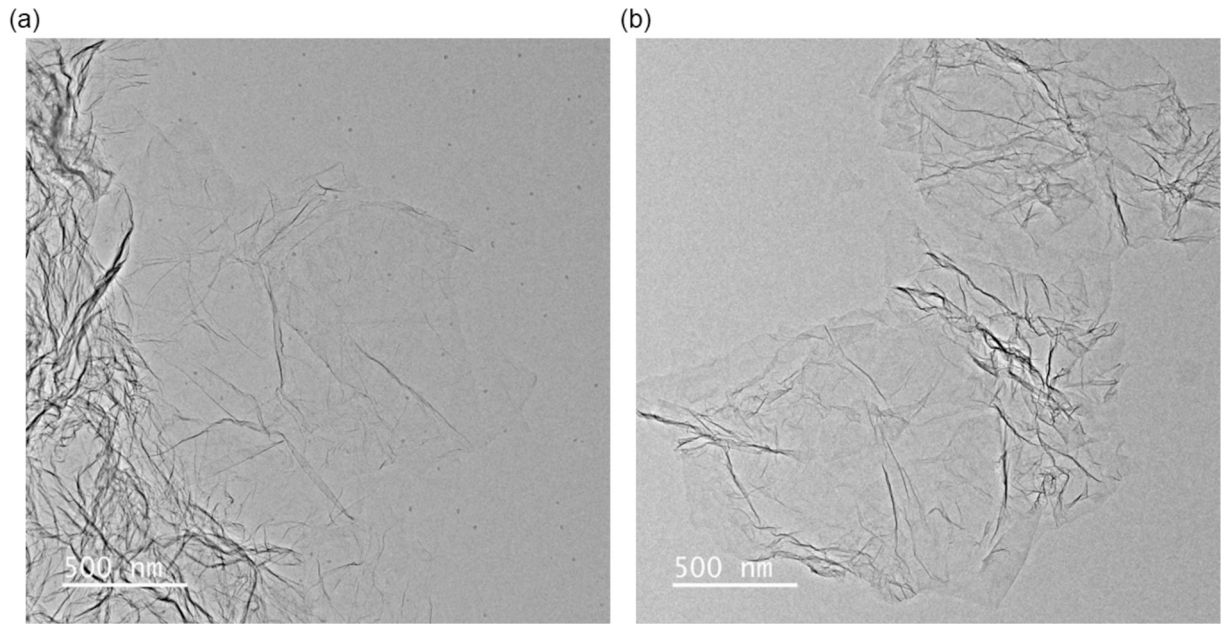

Fig. 2. TEM images of (a) pristine rGO and (b) rGO-S derivative.

from the graph that the benzenesulfonate derivative interacts with the cationic dye almost instantaneously, within 1 min of contact time, while pristine rGO takes more than 1 h to reach the equilibrium. The experimental data were additionally fitted with the pseudo-first and the pseudo-second-order kinetic models. The latter resulted in the highest value of correlation coefficient (R^2) and was therefore chosen for the calculation of the kinetic constant (k_2). Linear correlation for the pseudo-second-order kinetic model is reported in Fig. 5**b**. From the results in Table 3, $\mathbf{k_2}$ is two orders of magnitude higher for rGO-S than for rGO, confirming a faster adsorption process for the derivative. Moreover, the kinetic models are employed for the evaluation of the adsorption mechanism. In this case, the better fitting obtained with the pseudo-second-order kinetic model suggests that the process is most likely controlled by the chemisorption and that the rate of adsorption is directly proportional to the number of active sites on the surface of the adsorbent [56].

Kinetics is one of the most important means to evaluate the efficiency of an adsorption process and to compare different adsorbents. Considering adsorption studies with other graphene-based materials reported in the literature, rGO typically reaches an adsorption equilibrium in a time ranging from 30 min to a few hours [57–59], while with GO it commonly takes from 5 to 15 min, thus suggesting for GO a faster and more effective interaction with MB compared to rGO [24,60,61]. Similarly, other sulfonated graphene materials prepared by diazotization reaction reach equilibrium in approximately 30 min [41,42]. This behavior is most probably associated with the presence of oxygenated and/or sulfonated groups which act as additional adsorption sites with high affinity for cationic pollutants.

In the present study, rGO-S demonstrates much faster kinetics in comparison to all the above-mentioned graphene materials and derivatives, with instantaneous adsorption of the water pollutant, leaving a residual concentration lower than 1% in less than 1 min. Noteworthily, rGO-S adsorbs MB also faster than AC, which is the most widely employed material for dye adsorption. In fact, AC needs several hours to reach the equilibrium time, depending on the concentration of MB in solution [62,63]. This behavior is of particular interest from a practical perspective, as it has the potential to accelerate the overall water treatment process.

3.2.2. *Isotherm adsorption studies*

The study of adsorption isotherms, providing information about the adsorption capacity of the materials, was carried out by varying the initial amount of MB. The results reported in Fig. 6**a** show that the presence of benzenesulfonate functional groups increases the adsorption capacity of the nanomaterial by a factor of two. The experimental data were additionally fitted with Langmuir and Freundlich isotherm models and the results are reported in Table 4. The model that best matches the experimental data is the Langmuir isotherm (Fig. 6**b**), and the maximum adsorption capacity (q_m) extrapolated from data fitting resulted in 164 mg/g for pristine rGO and 326 mg/g for rGO-S. The Langmuir model is indicative that the adsorption mechanism of MB on rGO and rGO-S could be associated with a monolayer chemical adsorption process taking place at energetically equivalent sites and involving an electron or ion exchange between the adsorbent and the adsorbate [64].

The enhanced adsorption of the graphene derivative can be attributed to a dual effect resulting from the presence of sulfonated groups. Firstly, the negatively charged groups exhibit repulsion towards one another and interact favorably with water, resulting in the disaggregation of graphene sheets and the formation of a stable colloidal dispersion. Consequently, rGO-S possesses an increased number of exposed adsorption sites available for interaction with the pollutants in water. It is also possible that this phenomenon is the reason for the fastest kinetics. Furthermore, the negatively charged groups of rGO-S have the capacity to interact electrostatically with the positively charged pollutant, thereby further enhancing the adsorption capacity of rGO.

The adsorption capacity values reported in the literature for graphene-based materials vary considerably. This variation is attributable to differences in the graphitic starting material and in the functionalization or handling methodologies employed. For example, q_m values of 81–91 mg/g can be found for thermally reduced rGO [65], instead, q_m values of 122–159 mg/g are typically reached in the case of chemically reduced rGO [57,59,65]. Generally, the equilibrium dye uptake increases with increasing the oxidation degree of the nanostructure [61]. The maximum adsorption amount of MB on GO ranges from 17.3 to 1939 mg/g depending on the experimental conditions and the physico-chemical characteristics of the GO [13,22–24]. In general, functionalizations introducing sulfonate groups lead to an improvement in adsorption capacity. Kumari et al. [66] measured a q_m of 199 mg/g for GO sulfonated through amide bonds with 2-amino ethane sulfonic acid

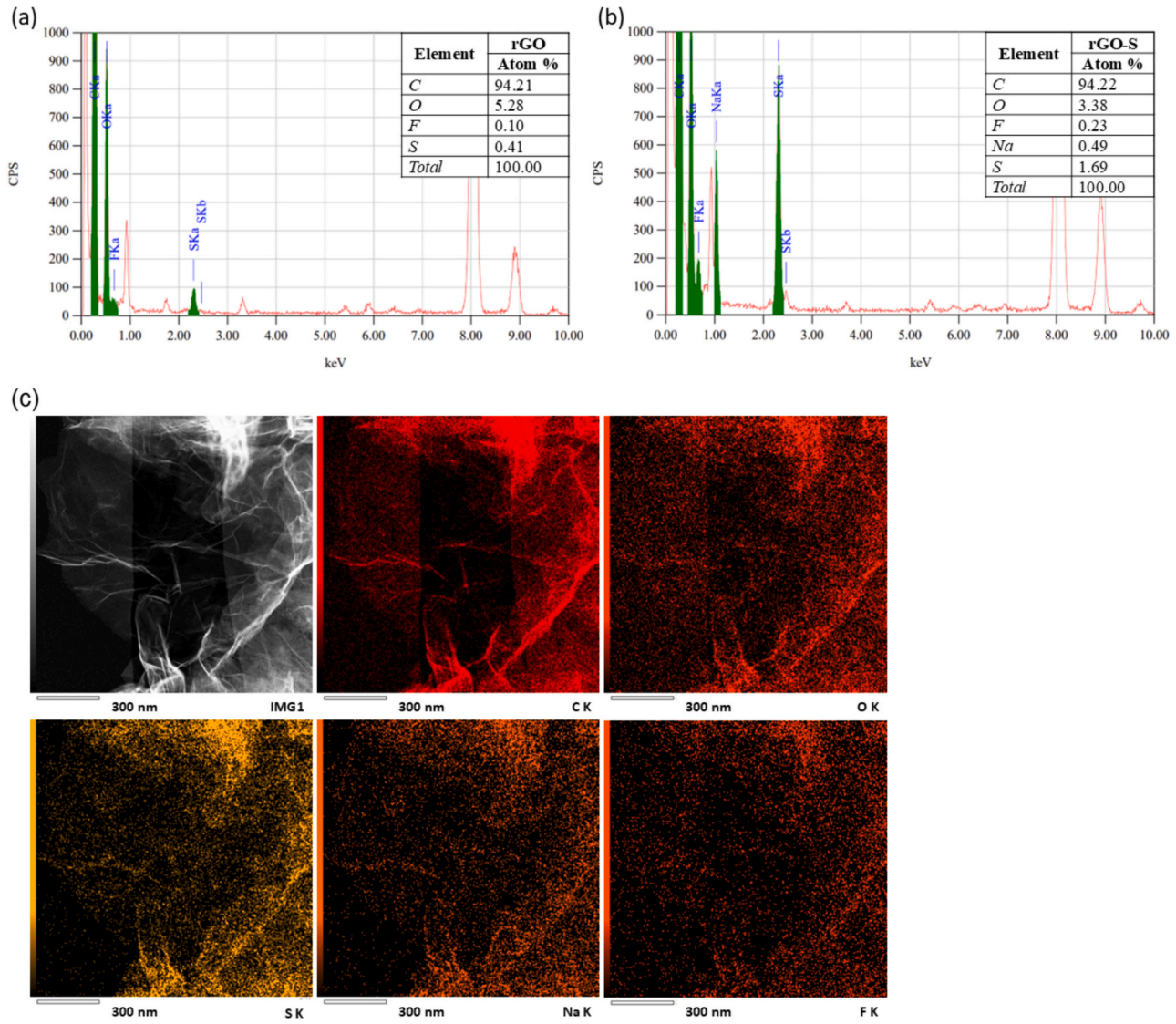

Fig. 3. EDX spectrum of (a) rGO and (b) rGO-S. The atomic percentage deducted from the spectrum is reported in the tables. (c) STEM image and the corresponding elemental map for C, O, S, Na and F elements of rGO-S.

(AESA). Shen et al. [41] determined a q_m of 906 mg/g for sulfonated rGO obtained through a diazotization reaction preceded and followed by GO reduction steps. As demonstrated by Wei et al. [42], a q_m of 2530 mg/g was found for sulfonated rGO obtained through the prereduction of GO and the subsequent diazotization. Conversely, a q_m of 2187 mg/g was determined for the aforementioned material, exhibiting an additional postreduction step after diazotization.

The adsorption capacity of rGO-S falls within the range of values reported in the literature for graphene-based materials. It is important to note that the derivatives under comparison were obtained from different starting materials and using different synthetic procedures, usually involving reduction steps from GO. Such disparities affect the presence of structural defects and of residual oxygen groups, thereby influencing the adsorption performance of the material.

On the other hand, rGO-S adsorbs MB with a capacity comparable to that of AC, which exhibits a q_m ranging from 253 to 769 mg/g, depending on the size of the particles and the surface area of the adsorbents [63,67,68].

Instead, compared with carbon nanotubes, rGO-S more than doubled the adsorption capacity of sulfonated MWCNT-S (150 mg/g) that we previously reported [36]. This can be ascribed to the larger surface area of rGO compared to multi-walled CNT, respectively 400–1000 m^2/g and > 233 m^2/g. These results highlight how relevant both the available surface area and the surface functionalization of carbon nanostructures are in the design of nanocarbon-based pollutant adsorbents.

3.2.3. *Desorption experiments*

The desorption of MB was investigated with the purpose of examining the feasibility of regenerating and reusing the saturated adsorbent. Indeed, rGO-S is functionalized with sulfonate groups, just like resins in strong cation exchange columns that are regenerated by washing with salts. This approach is also reported in the literature specifically for electrostatically charged dyes. For example, a saturated NaCl solution in water was used for the removal of anionic dyes form a poly(N,N0-methylene-bis(1-(3-vinylimidazolium)) chloride) column [69], or a 1% NaCl solution was used for the removal of a cationic dyes mixture from a starch-based ion exchange resin synthesized by copolymerizing raw starch with sodium methallyl sulfonate and styrene [70]. Different concentrations and bed volumes of NaCl, HCl and NaOH solutions were also employed in the desorption of pharmaceuticals from a polymeric anion exchange resin, and better desorption capacity was achieved by enhancing bed volumes rather than salts concentration [71].

We ourselves have reported on the remarkable effectiveness of regeneration of MWCNT-S as adsorbent for MB, through ion exchange

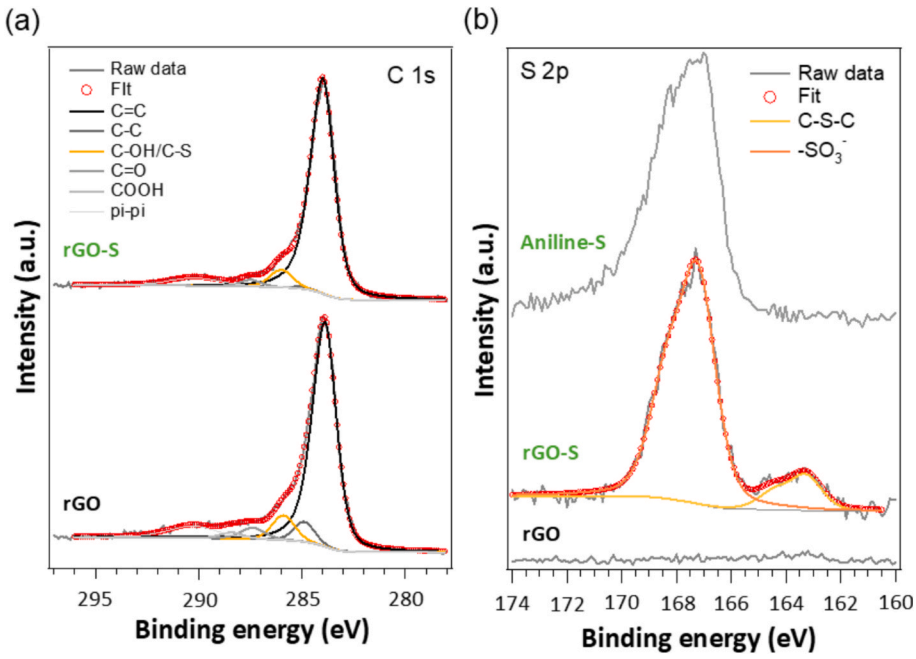

Fig. 4. XPS spectra and their deconvolution in chemical shifted components of (a) C 1s and (b) S 2p photoelectron signals in pristine rGO and functionalized rGO-S. The S 2p spectrum of sodium sulfanilate (Aniline-S) has been added as reference.

Table 1
Analysis of the XPS results. For each sample, the binding energy and the at.% of the C 1s components is reported, as well as the atomic C:O:S ratio.

Sample	C sp^2	C sp^3	C-OH/ C-S	Carbonyl groups	Carboxylic groups	Atomic C:S:O ratio
rGO	284.0 eV 81.0%	285.0 eV 5.5%	286.0 eV 7.4%	287.4 eV 3.9%	288.4 eV 2.2%	95.6: 0: 4.4
rGO-S	284.0 eV 91.2%	285.0 eV 0.7%	286.0 eV 7.4%	287.5 eV 6.0%	–	78.8: 5.2: 16.0

Table 2
Analysis of the XPS results. The binding energy and the at.% of the S 2p components is reported.

Sample	C-S-C	$-SO_3^-$
rGO-S	163.2 eV 12.4%	167.2 eV 87.6%

with NaCl solutions [36]. Therefore, following a similar approach, rGO-S was first tested for the adsorption of MB in different ionic strength conditions (**Fig. S6**) demonstrating that the Na^+ ions could compete with MB for rGO-S adsorption sites. Then, based on the literature and the ion-exchange hypothesis, rGO-S was tested for MB desorption with different salt concentrations ranging from 0.5 M to saturated NaCl solutions, different volumes of solution of 25 and 40 mL and different contact times of 1 h and 24 h. Moreover, ethanol has been extensively used in the literature for MB removal from GO [66], graphene composites [72] and AC [73]. Thus, ethanol was also tested as desorbing solvent varying contact times from 1 to 24 h.

rGO-S was first saturated with a MB solution and then treated with different regeneration solutions, see details in section 2.6.3. Fig. 7**a** summarizes the results obtained with the different tested conditions (experiments D01-D09) as the percentage of MB desorbed versus the adsorbed quantity. The treatment with aqueous NaCl 1 M is the most efficient, reaching a desorption of 78% with 25 mL of solution already in 1 h (D04). Changing the volume of desorption solution from 25 to 40 mL (D05) slightly increases the regeneration up to 82%. This suggests the possibility of completely regenerating the material using higher volumes and could be easily achieved in flow systems. On the other hand, increasing the contact time from 1 to 24 h (D06) lead to a modest improvement, suggesting that equilibrium with the solution is reached very quickly within approximately 1 h of contact. The results also show that too low salt concentrations (D03) do not guarantee complete regeneration of the adsorption sites, but on the other hand too high concentrations of NaCl (D07, D08) hamper the release of MB molecules into the solution, probably because dye solubility decreases with increasing ionic strength. Moreover, ethanol showed a much lower ability to remove MB from the adsorbent material compared to the salt solution even with 24 h of contact time (D01, D02). This is a further confirmation that the mechanism of pollutant adsorption is mainly electrostatic. Finally, as a control experiment, the material was also treated with Milli-Q water (D09), resulting in the removal of only 1% of adsorbed MB after 1 h, thus supporting an ion exchange mechanism of regeneration of the material, when observed.

From a practical point of view, the use of NaCl as desorbing agent can be very advantageous because it is cheap, stable, non-hazardous and environmentally friendly. Moreover, it allows the regeneration of the starting material without affecting its structure or properties, as could occur with oxidative or biological processes.

Additionally, a different approach based on subsequent desorption steps was tested. rGO-S was first treated with a desorption solution, then recovered through centrifuge, dried and subsequently treated with another desorption solution to encourage further release of MB; the results are reported in Fig. 7**b**. One sample (D10) was double treated using 20 mL of 1 M aqueous NaCl solution and the percentage of MB desorbed increased from 62% to 70%. Another sample (D11) was double treated with 40 mL of 1 M aqueous NaCl solution and the percentage of MB desorbed increased from 82% to 92%. The addition of a subsequent desorption step thus resulted in an increase in desorption capacity of approximately 10% in both cases. An additional experiment (D12) was conducted by treating the sample first with ethanol to remove the physiosorbed MB and then with aqueous NaCl solutions to remove the remaining chemisorbed MB by ion exchange. As reported in the graph, ethanol was able to remove 15% of MB adsorbed on the nanostructure,

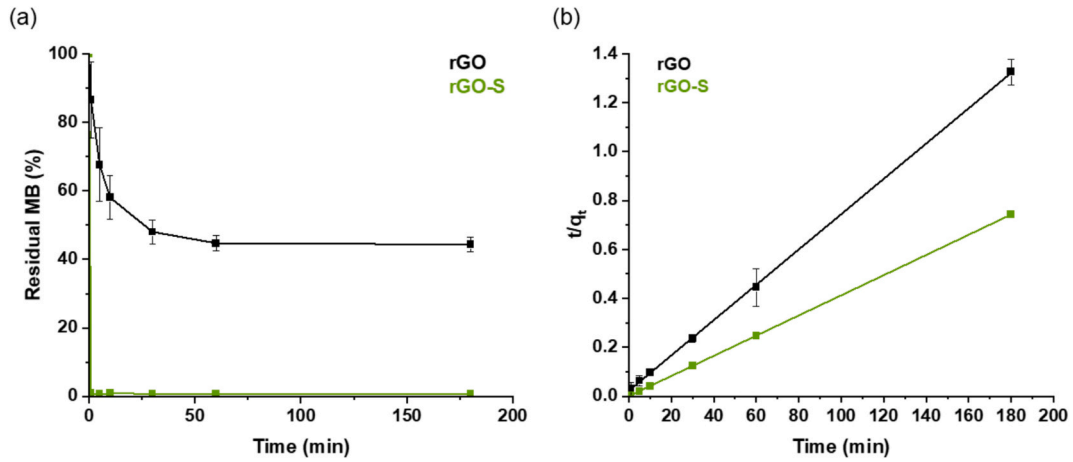

Fig. 5. (a) Percentage residual concentration of MB in solution as a function of time for rGO and rGO-S, (b) Pseudo-second-order kinetic plots for the adsorption of MB on rGO and rGO-S.

Table 3
Kinetic parameters derived from the pseudo-first-order and pseudo-second-order kinetic models.

Kinetic Parameters	Values	
	rGO	rGO-S
	Pseudo-first-order kinetic model	
R^2	0.9933	0.4794
k_1 (1/min)	–	–
	Pseudo-second-order kinetic model	
R^2	0.9999	1
k_2 (g/(min·mg))	$2.3 \cdot 10^{-3}$	$1.8 \cdot 10^{-1}$
q_{eq} (mg/g)	138.5	242.1

and with two subsequent additions of 1 M aqueous NaCl, 92% desorption was achieved.

3.2.4. Regeneration and reusability experiments

Multiple adsorption and desorption cycles were performed to investigate the cyclability of the process for the recovery and reuse of the adsorbent. This is an important study for evaluating the cost of the process and applicability of adsorbents [74], as well as for ensuring the possibility of using the adsorbent materials to concentrate pollutants in a smaller water volume, thereby facilitating subsequent water purification treatments. In the specific case in which desorption is carried out in a high-salinity solution, literature reports examples of advanced oxidation processes in which the presence of NaCl is advantageous for MB degradation [75].

rGO-S was tested for three adsorption/desorption cycles using the desorption condition D12. The details on experimental procedures are reported in section 2.6.4. The desorption effectiveness of MB was calculated as the amount of MB desorbed versus the amount of MB adsorbed onto rGO-S. As reported in Fig. 7**c**, the percentage of MB

Table 4
Isotherm parameters calculated using the Langmuir and Freundlich models.

Adsorption Isotherm Parameters	Values	
	rGO	rGO-S
	Langmuir Isotherm	
R^2	0.9716	0.9978
K_L (L/mg)	$7.5 \cdot 10^{-1}$	$9.6 \cdot 10^{-1}$
q_m (mg/g)	163.9	325.7
	Freundlich Isotherm	
R^2	0.2038	0.8819
K_F	–	–

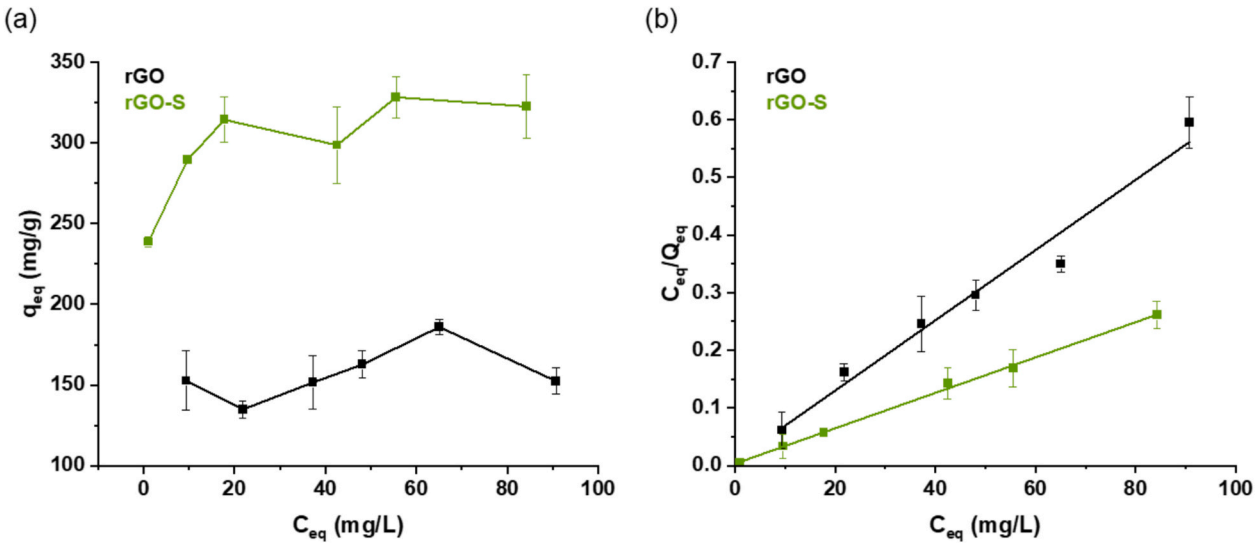

Fig. 6. (a) Equilibrium adsorption capacity q_{eq} as a function of the equilibrium concentration of MB C_{eq} after adsorption on rGO and rGO-S, (b) Langmuir isotherm plots for the adsorption of MB on rGO and rGO-S.

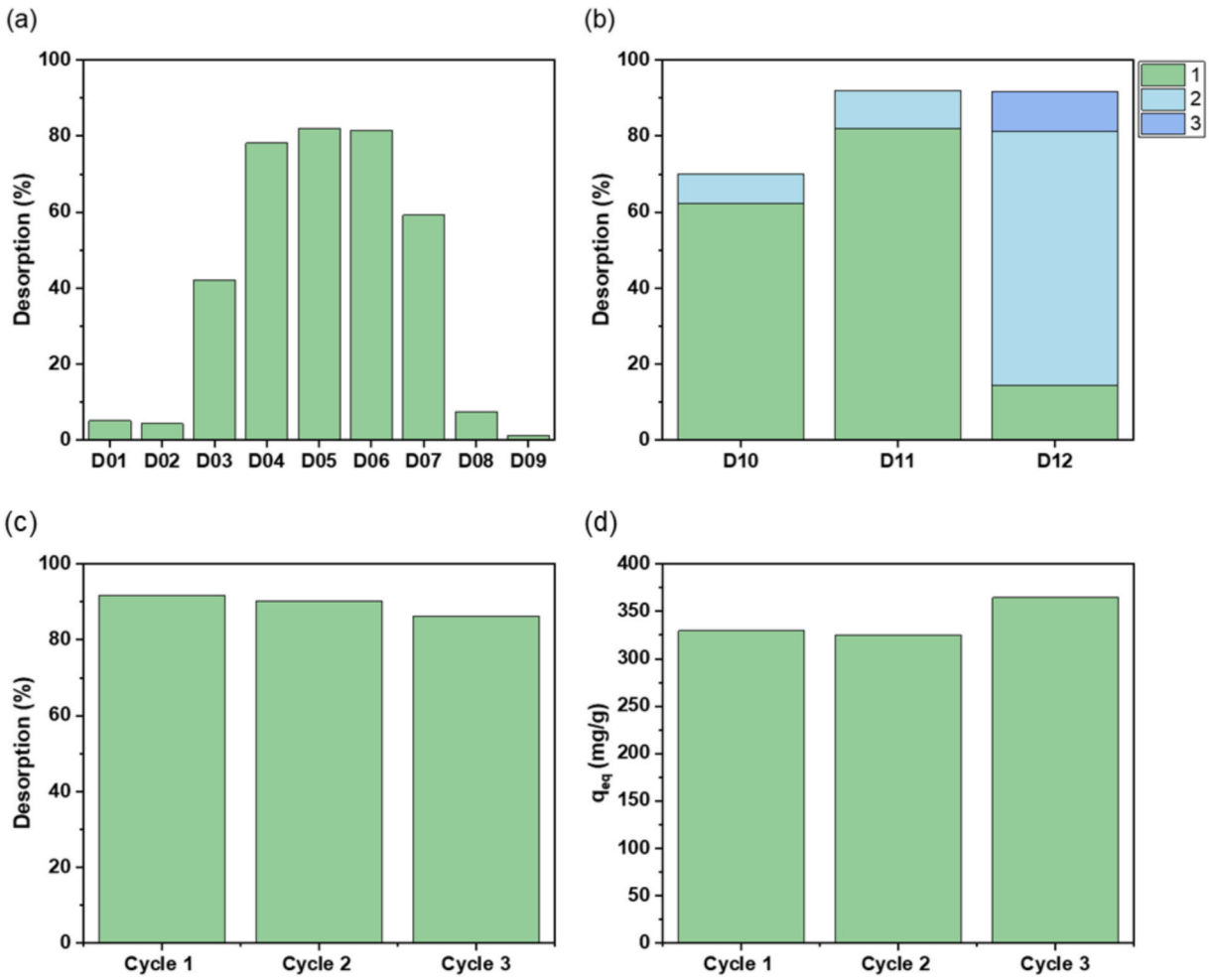

Fig. 7. Percentage of desorbed MB from rGO-S material using different regeneration conditions through (a) single desorption step and (b) multiple desorption steps. (c) Percentage of desorbed MB and (d) rGO-S adsorption capacity in three subsequent adsorption/desorption cycles.

removal decreased by 2% between the first and second cycle and by 4% between the second and third cycle, while still remaining above 85%. The regeneration rate of rGO-S is in agreement with other studies on MB desorption that can be found in the literature for modified GO [61,66].

Moreover, the adsorption capacities of rGO-S for the three cycles were compared and reported in Fig. 7**d**. The calculated q_{eq} values are 330, 325 and 365 mg/g for the first, second and third cycle, respectively. The findings demonstrate that the MB desorption is effective to a significant extent, and that the material adsorption efficacy remains consistent in subsequent cycles.

3.2.5. *Selectivity experiment*

Another interesting and useful object of study on graphene derivatives as adsorbents is the selectivity in multi-component mixtures of pollutants. Here, pristine graphene and rGO-S were tested for adsorption of three different dyes: MB, MO and RhB, see Fig. 8**a** for the schematic representation of the molecules. These three chemicals are well-known and widely used dyes in industry and exhibit different molecular structures that could specifically interact with graphene materials. In particular, they feature extended sp^2 structures that could possibly give rise to π-π stacking with graphene surface and different charged groups. In water, MB is positively charged, while MO and RhB are pH colorimetric indicators and exist in equilibrium between two molecular structures upon protonation. MO (pKa = 3.4) [76] is protonated and orange-colored below pH 3.1, whereas it is deprotonated and yellow-colored above pH 4.4; on the other hand, RhB (pKa for the aromatic carboxylic acid group present on the rhodamine B is ~4.2) [77] displays the open form at pH below 5 when it is zwitterionic and pink-colored, otherwise at higher pH values the closed form prevails, and it becomes uncharged and colorless. The adsorption experiments were performed in water under normal atmospheric conditions, at pH = 5.8, therefore, MO was in its yellow deprotonated form and RhB was present in both open and closed forms.

It is worth noting that the selectivity experiments were carried out in tap water, in order to better mimic realistic aqueous conditions in the presence of dissolved inorganic ions. These experiments were performed with a low pollutant concentration (5 mg/L) to ensure that the adsorption sites on the nanostructures were not saturated. Fig. 8**b** reports the removal percentage of pollutants for the two different graphene materials. As expected, pristine rGO adsorbs all dyes indistinctly, showing no selectivity toward a specific compound. Instead, rGO-S clearly shows a preferential interaction with MB and a lower adsorption capacity towards other compounds. Such behavior may be useful for the detection of organic cationic pollutants in solution and their recovery for possible reuse, in the case of expensive or critical compounds. As illustrated in Fig. 8**c**, the shift in color of the mixture of dyes before and after treatment with the adsorbents supports the observation that only rGO-S selectively removed MB, leaving an orange-pink color resulting from the other two dyes.

While previously mentioned works on sulfonated grafene materials do not report on selectivity [38,41,42], studies on preferential adsorption were carried on in the past on GO and cellulose-based composite materials containing sulfonated GO [60]. Our findings are in agreement with those works, which found higher removal efficiencies for positively

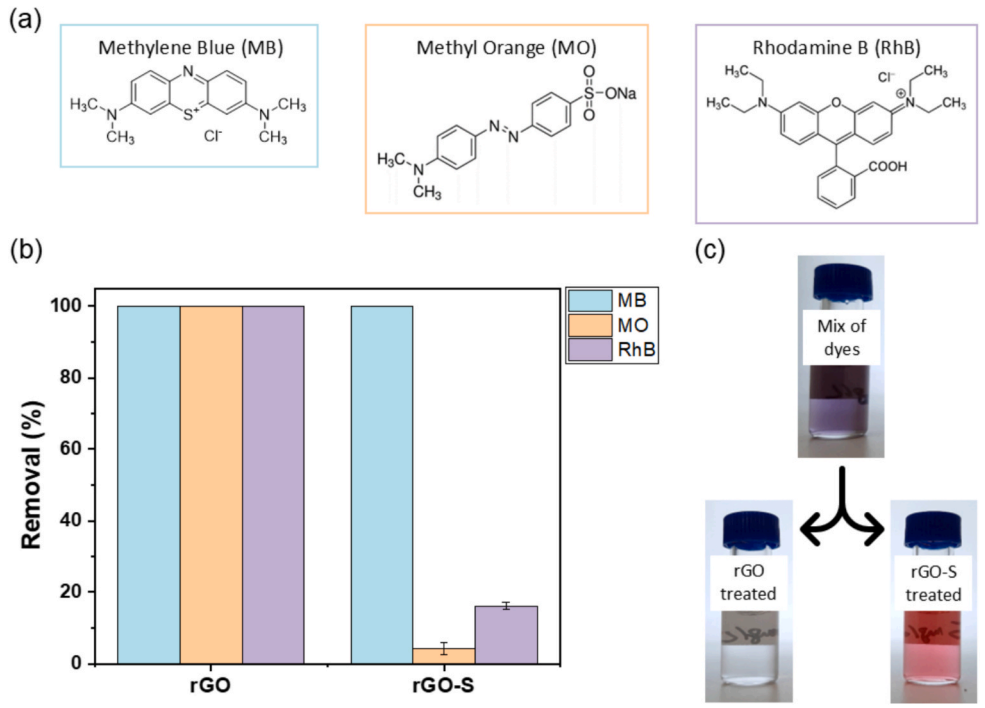

Fig. 8. (a) Molecular structure of MB, MO and RhB dyes. (b) Percentage of dyes removal from the mixture for rGO and rGO-S. (c) Pictures of the dye mixture before and after treatment with rGO and rGO-S.

charged dyes such as MB, ascribing this selectivity to the negatively charged groups of the adsorbent.

3.3. Comparison of MB removal with different sulfonated graphene adsorbents reported in literature

Finally, the present work also demonstrates efficient regeneration of the adsorbent through ion-exchange treatment, enabling repeated adsorption–desorption cycles with high recovery efficiency. These features highlight the potential of the covalently functionalized graphene material for practical water purification applications.

As summarized in Table 5, compared with previously reported sulfonated graphene materials, obtained with different chemistry or procedures, rGO-S exhibits lower adsorption capacity but significantly faster adsorption kinetics. Indeed, while adsorption capacities reported in the literature for sulfonated graphene materials are typically achieved with equilibrium times ranging from several minutes to hours, the adsorbent developed in this work reaches equilibrium in less than one minute. This remarkable behavior can be attributed to the excellent dispersion of the functionalized graphene sheets and the high accessibility of adsorption sites, enabling strong electrostatic interactions between sulfonate groups and cationic dye molecules. Such interactions are confirmed by our selectivity and desorption studies, not reported in previous works, with appealing perspectives for application.

4. Conclusions and perspectives

In the present study, the graphene based derivative rGO-S was synthesized and characterized, confirming the presence of sulphonate groups and their role in promoting dispersion in water. We have demonstrated that the resulting larger available surface area and the presence of negative charges boost adsorption of MB providing at the same time extended adsorption sites and specific electrostatic interactions with the positively charged contaminant, in comparison with pristine rGO.

Thanks to such features, rGO-S resulted extremely fast in adsorbing MB, removing a significant amount of MB in less than 1 min of contact time, thus outperforming, in terms of kinetics, not only other graphene materials but also the widely used AC.

The role of electrostatic interactions in the adsorption was confirmed by regeneration studies based on treatments of MB-saturated rGO-S with different desorption solutions. Indeed, the treatment with 1 M aqueous NaCl was the most efficient, whereas ethanol exhibited a much lower desorption activity. Based on these observations, we explored the possibility to further push regeneration by testing a few sequences of treatments with ethanol and saline aqueous solutions, leading to desorption outcomes up to 92%. In addition, repeated adsorption and desorption cycles assessed the reusability and durability of the material.

Alongside elucidating the adhesion mechanism, these results provide significant perspectives for practical implementation, involving the reuse of the adsorbent material and an easier degradation of the pollutant or, when particularly relevant, its recovery.

Finally, rGO-S demonstrated a selective tendency towards MB adsorption in a mixture of three dyes, thus disclosing the possibility to consider rGO-S for the recovery and subsequent reuse of chemicals with structural features similar to MB, allowing a circular economy approach.

Table 5
Comparison of MB removal with different sulfonated graphene adsorbents reported in literature.

Material	Functionalization method	q_m (mg/g)	Equilibrium time	Regeneration	Reference
Sulfonated graphene nanosheets	Diazotization of GO + reduction	~900	30 min	no data	Ref. [41]
Sulfonated graphene materials	Hydrothermal sulfonation	~600	~1 h	no data	Ref. [38]
Reduced Sulfonated GO	Diazotization of GO + reduction	~2000	~30 min	no data	Ref. [42]
rGO-S (this work)	Covalent diazonium grafting on rGO	~320	< 1 min	92% recovery	This work

CRediT authorship contribution statement

Ludovica Ceroni: Writing – original draft, Investigation, Data curation. **Samuel Pressi:** Methodology, Investigation. **Laura Calvillo:** Writing – original draft, Investigation, Data curation. **Ester Marotta:** Writing – review & editing, Methodology, Funding acquisition, Conceptualization. **Enzo Menna:** Writing – review & editing, Supervision, Methodology, Funding acquisition, Conceptualization.

Declaration of competing interest

The authors declare that they have no known competing financial interests or personal relationships that could have appeared to influence the work reported in this paper.

Acknowledgements

Financial support from the University of Padova, Italy, is acknowledged by EM, LCa for grant P-DiSC#05BIRD2021-UNIPD (CORDER). PhD fellowship of L.Ce. was financed by PON 2014-2020 (National Operative Program 'Research and Innovation'), Italy, D.M. n. 1061, August 10th 2021, Action IV.5.

Appendix A. Supplementary data

Supplementary data to this article can be found online at https://doi.org/10.1016/j.apsusc.2026.167074.

Data availability

The data supporting this article have been included as part of the Supplementary Information.

References

[1] K.K. Chenab, B. Sohrabi, A. Jafari, S. Ramakrishna, Water treatment: functional nanomaterials and applications from adsorption to photodegradation, Mater. Today Chem. 16 (2020) 100262.
[2] S. Manikandan, N. Karmegam, R. Subbaiya, G.K. Devi, R. Arulvel, B. Ravindran, M. K. Awasthi, Emerging nano-structured innovative materials as adsorbents in wastewater treatment, Bioresour. Technol. 320 (2021) 124394.
[3] A.M. Awad, R. Jalab, A. Benamor, M.S. Nasser, M.M. Ba-Abbad, M. El-Naas, A. W. Mohammad, adsorption of organic pollutants by nanomaterial-based adsorbents an overview, J. Mol. Liq. 301 (2020) 112335.
[4] Jain, M.; Khan, S. A.; Pandey, A.; Pant, K. K.; Ziora, Z. M.; Blaskovich, M. A. Instructive Analysis of Engineered Carbon Materials for Potential Application in Water and Wastewater Treatment. *Science of the Total Environment* **2021**, *793*, 148583.
[5] R. Gusain, N. Kumar, S.S. Ray, Recent advances in carbon nanomaterial-based adsorbents for water purification, Coord. Chem. Rev. 405 (2020) 213111.
[6] N. Madima, S. Mishra, I. Inamuddin, A. Mishra, Carbon-based nanomaterials for remediation of organic and inorganic pollutants from wastewater a review, Environ. Chem. Lett. 18 (2020) 1169–1191.
[7] Madhura, L.; Singh, S.; Kanchi, S.; Sabela, M.; Bisetty, K.; Inamuddin. Nanotechnology-Based Water Quality Management for Wastewater Treatment. *Environmental Chemistry Letters* **2019**, *17*, 65–121.
[8] I. Ali, X. Mbianda, A. Burakov, E. Galunin, I. Burakova, E. Mkrtchyan, A. Tkachev, V. Grachev, et al., Graphene based adsorbents for remediation of noxious pollutants from wastewater, Environ. Int. 127 (2019) 160–180.
[9] N. Baig, M. Sajid, T.A. Saleh, et al., Graphene-based adsorbents for the removal of toxic organic pollutants a review, J. Environ. Manag. 244 (2019) 370–382.
[10] V.I. Isaeva, M.D. Vedenyapina, A.Y. Kurmysheva, D. Weichgrebe, R.R. Nair, N.P. T. Nguyen, L.M. Kustov, Modern carbon–based materials for adsorptive removal of organic and inorganic pollutants from water and wastewater, Molecules 26 (21) (2021) 6628.
[11] J.-G. Yu, L.-Y. Yu, H. Yang, Q. Liu, X.-H. Chen, X.-Y. Jiang, X.-Q. Chen, F.-P. Jiao, Graphene nanosheets as novel adsorbents in adsorption, preconcentration and removal of gases, organic compounds and metal ions, Sci. Total Environ. 502 (2015) 70–79, https://doi.org/10.1016/j.scitotenv.2014.08.077.
[12] L. Ji, W. Chen, Z. Xu, S. Zheng, D. Zhu, Graphene nanosheets and graphite oxide as promising adsorbents for removal of organic contaminants from aqueous solution, J. Environ. Qual. 42 (1) (2013) 191–198.
[13] Y. Li, Q. Du, T. Liu, X. Peng, J. Wang, J. Sun, Y. Wang, S. Wu, Z. Wang, Y. Xia, et al., Comparative study of methylene blue dye adsorption onto activated carbon graphene oxide, and carbon nanotubes, Chem. Eng. Res. Design 91 (2) (2013) 361–368.
[14] Gul, A.; Ma'amor, A.; Khaligh, N. G.; Julkapli, N. M. Recent Advancements in the Applications of Activated Carbon for the Heavy Metals and Dyes Removal. *Chemical Engineering Research and Design* **2022**, *186*, 276–299.
[15] G. Ersan, O.G. Apul, F. Perreault, T. Karanfil, Adsorption of organic contaminants by graphene nanosheets: a review, Water Res. 126 (2017) 385–398.
[16] M.-M.-A. Aslam, H.-W. Kuo, W. Den, M. Usman, M. Sultan, H. Ashraf, Functionalized carbon nanotubes (CNTs) for water and wastewater treatment preparation to application, Sustainability 13 (10) (2021) 5717.
[17] S. Khaliha, T.D. Marforio, A. Kovtun, S. Mantovani, A. Bianchi, M.L. Navacchia, M. Zambianchi, L. Bocchi, N. Boulanger, A. Iakunkov, et al., Defective graphene nanosheets for drinking water purification: adsorption mechanism, performance, and recovery, FlatChem 29 (2021) 100283.
[18] V.K. Garg, M. Amita, R. Kumar, R. Gupta, Basic Dye (methylene blue) removal from simulated wastewater by adsorption using Indian rosewood sawdust: a timber industry waste, Dyes Pigm. 63 (3) (2004) 243–250.
[19] Koyuncu, H.; Kul, A. R. Removal of Methylene Blue Dye from Aqueous Solution by Nonliving Lichen (Pseudevernia Furfuracea (L.) Zopf.), as a Novel Biosorbent. *Applied Water Science* **2020**, *10* (2), 72.
[20] S. Parakala, S. Moulik, S. Sridhar, Effective separation of methylene blue dye from aqueous solutions by integration of micellar enhanced ultrafiltration with vacuum membrane distillation, Chem. Eng. J. 375 (2019) 122015.
[21] Khan, I.; Saeed, K.; Zekker, I.; Zhang, B.; Hendi, A. H.; Ahmad, A.; Ahmad, S.; Zada, N.; Ahmad, H.; Shah, L. A.; others. Review on Methylene Blue: Its Properties, Uses, Toxicity and Photodegradation. *Water* **2022**, *14* (2), 242.
[22] G. Ramesha, A.V. Kumara, H. Muralidhara, S. Sampath, Graphene and graphene oxide as effective adsorbents toward anionic and cationic dyes, J. Colloid Interface Sci. 361 (1) (2011) 270–277.
[23] S.-T. Yang, S. Chen, Y. Chang, A. Cao, Y. Liu, H. Wang, Removal of methylene blue from aqueous solution by graphene oxide, J. Colloid Interface Sci. 359 (1) (2011) 24–29.
[24] W. Zhang, C. Zhou, W. Zhou, A. Lei, Q. Zhang, Q. Wan, B. Zou, Fast and considerable adsorption of methylene blue dye onto graphene oxide, Bull. Environ. Contam. Toxicol. 87 (2011) 86–90.
[25] T. Wu, X. Cai, S. Tan, H. Li, J. Liu, W. Yang, Adsorption characteristics of acrylonitrile, p-toluenesulfonic acid, 1-naphthalenesulfonic acid and methyl blue on graphene in aqueous solutions, Chem. Eng. J. 173 (1) (2011) 144–149.
[26] J. Xiao, W. Lv, Z. Xie, Y. Tan, Y. Song, Q. Zheng, Environmentally friendly reduced graphene oxide as a broad-spectrum adsorbent for anionic and cationic dyes via π–π interactions, J. Mater. Chem. A 4 (31) (2016) 12126–12135, https://doi.org/10.1039/C6TA04119A.
[27] F. Tunioli, T.D. Marforio, L. Favaretto, S. Mantovani, A. Pintus, A. Bianchi, A. Kovtun, M. Agnes, V. Palermo, M. Calvaresi, et al., Chemical tailoring of β-cyclodextrin-graphene oxide for enhanced per-and polyfluoroalkyl substances (PFAS) adsorption from drinking water, Chemistry–a European Journal 29 (60) (2023) e202301854.
[28] S. Mantovani, T.D. Marforio, S. Khaliha, A. Pintus, A. Kovtun, F. Tunioli, L. Favaretto, A. Bianchi, M.L. Navacchia, V. Palermo, M. Calvaresi, M. Melucci, Amino acid-driven adsorption of emerging contaminants in water by modified graphene oxide nanosheets, Environ. Sci. Water Res. Technol. 9 (4) (2023) 1030–1040, https://doi.org/10.1039/D2EW00871H.
[29] C.A. Dyke, J.M. Tour, Covalent functionalization of single-walled carbon nanotubes for materials applications, J. Phys. Chem. A 108 (51) (2004) 11151–11159, https://doi.org/10.1021/jp046274g.
[30] L. Rodríguez-Pérez, M.Á. Herranz, N. Martín, The chemistry of pristine graphene, Chem. Commun. 49 (36) (2013) 3721, https://doi.org/10.1039/c3cc38950b.
[31] E. Bekyarova, M.E. Itkis, P. Ramesh, C. Berger, M. Sprinkle, W.A. De Heer, R. C. Haddon, Chemical modification of epitaxial graphene: spontaneous grafting of aryl groups, J. Am. Chem. Soc. 131 (4) (2009) 1336–1337, https://doi.org/10.1021/ja8057327.
[32] C.A. Mitchell, J.L. Bahr, S. Arepalli, J.M. Tour, R. Krishnamoorti, Dispersion of functionalized carbon nanotubes in polystyrene, Macromolecules 35 (23) (2002) 8825–8830, https://doi.org/10.1021/ma020890y.
[33] J.L. Hudson, M.J. Casavant, J.M. Tour, Water-soluble, exfoliated, nonroping single-wall carbon nanotubes, J. Am. Chem. Soc. 126 (36) (2004) 11158–11159, https://doi.org/10.1021/ja0467061.
[34] C.A. Dyke, J.M. Tour, Overcoming the insolubility of carbon nanotubes through high degrees of sidewall functionalization, Chemistry A European J 10 (4) (2004) 812–817, https://doi.org/10.1002/chem.200305534.
[35] M.E. Lipińska, S.L.H. Rebelo, M.F.R. Pereira, J.A.N.F. Gomes, C. Freire, J. L. Figueiredo, New insights into the functionalization of multi-walled carbon nanotubes with aniline derivatives, Carbon 50 (9) (2012) 3280–3294, https://doi.org/10.1016/j.carbon.2011.12.018.
[36] L. Ceroni, S. Benazzato, S. Pressi, L. Calvillo, E. Marotta, E. Menna, Enhanced adsorption of methylene blue dye on functionalized multi-walled carbon nanotubes, Nanomaterials 14 (6) (2024) 522, https://doi.org/10.3390/nano14060522.
[37] Stocco, E.; Barbon, S.; Ceroni, L.; Confalonieri, M.; Pulzato, G.; Pressi, S.; D'Osualdo, A.; Contran, M.; Boscolo-Berto, R.; Tiengo, C.; Todros, S.; Pavan, P. G.; Macchi, V.; De Caro, R.; Calvillo, L.; Menna, E.; Porzionato, A. Partially Oxidized Polyvinyl Alcohol + Functionalized Water Soluble Multiwalled Carbon Nanotubes: A New Conductive Nanocomposite Material with Promising Implications for Neuroregeneration. *Journal of Science: Advanced Materials and Devices* **2024**, *9* (3), 100762. doi:10.1016/j.jsamd.2024.100762.

[38] S. A.; . R. N.; . S. M.; . S. C. Sulfonated Graphene – An Efficient Cationic Dye Adsorbent in Aqueous Solution. *Advanced Materials Proceedings* **2021**, *2* (11), 704–710. doi:10.5185/amp.2018/728.

[39] Y. Si, E.T. Samulski, Synthesis of water soluble graphene, Nano Lett. 8 (6) (2008) 1679–1682, https://doi.org/10.1021/nl080604h.

[40] G. Zhao, L. Jiang, Y. He, J. Li, H. Dong, X. Wang, W. Hu, Sulfonated graphene for persistent aromatic pollutant management, Adv. Mater. 23 (34) (2011) 3959–3963, https://doi.org/10.1002/adma.201101007.

[41] Y. Shen, B. Chen, Sulfonated graphene nanosheets as a superb adsorbent for various environmental pollutants in water, Environ. Sci. Technol. 49 (12) (2015) 7364–7372, https://doi.org/10.1021/acs.est.5b01057.

[42] M. Wei, H. Chai, Y. Cao, D. Jia, Sulfonated graphene oxide as an adsorbent for removal of Pb^{2+} and methylene blue, J. Colloid Interface Sci. 524 (2018) 297–305, https://doi.org/10.1016/j.jcis.2018.03.094.

[43] Lagergren, S. About the Theory of So-Called Adsorption of Soluble Substances. **1898**.

[44] Al-Ghouti, M. A.; Da'ana, D. A. Guidelines for the Use and Interpretation of Adsorption Isotherm Models: A Review. *Journal of hazardous materials* **2020**, *393*, 122383.

[45] P. Salice, E. Fabris, C. Sartorio, D. Fenaroli, V. Figà, M.P. Casaletto, S. Cataldo, B. Pignataro, E. Menna, An insight into the functionalisation of carbon nanotubes by diazonium chemistry: towards a controlled decoration, Carbon 74 (2014) 73–82, https://doi.org/10.1016/j.carbon.2014.02.084.

[46] J.L. Bahr, J. Yang, D.V. Kosynkin, M.J. Bronikowski, R.E. Smalley, J.M. Tour, Functionalization of carbon nanotubes by electrochemical reduction of aryl diazonium salts: a bucky paper electrode, J. Am. Chem. Soc. 123 (27) (2001) 6536–6542, https://doi.org/10.1021/ja010462s.

[47] S. Eigler, C. Dotzer, F. Hof, W. Bauer, A. Hirsch, Sulfur species in graphene oxide, Chemistry A European J 19 (29) (2013) 9490–9496, https://doi.org/10.1002/chem.201300387.

[48] T. Okpalugo, P. Papakonstantinou, H. Murphy, J. McLaughlin, N. Brown, High resolution XPS characterization of chemical functionalised MWCNTs and SWCNTs, Carbon 43 (1) (2005) 153–161.

[49] M.C. Biesinger, Accessing the robustness of adventitious carbon for charge referencing (Correction) purposes in XPS analysis: insights from a multi-user facility data review, Appl. Surf. Sci. 597 (2022) 153681.

[50] J. Sun, J.-Y. Hwang, P. Jankowski, L. Xiao, J.S. Sanchez, Z. Xia, S. Lee, A. V. Talyzin, A. Matic, V. Palermo, et al., Critical role of functional groups containing N, S, and O on graphene surface for stable and fast charging Li-S batteries, Small 17 (17) (2021) 2007242.

[51] L. Ceroni, T. Feng, L. Calvillo, S. Casalini, P. Van Rijn, E. Menna, Quaternary ammonium-functionalized carbon nanotubes/alginate nanocomposite hydrogels support myoblast growth and differentiation, J. Mater. Chem. B 13 (27) (2025) 8105–8120, https://doi.org/10.1039/D5TB00601E.

[52] J. Amaro-Gahete, A. Benítez, R. Otero, D. Esquivel, C. Jiménez-Sanchidrián, J. Morales, Á. Caballero, F.J. Romero-Salguero, A comparative study of particle size distribution of graphene nanosheets synthesized by an ultrasound-assisted method, Nanomaterials 9 (2) (2019) 152.

[53] N.S. Andryushina, O.L. Stroyuk, I.B. Yanchuk, A.V. Yefanov, A dynamic light scattering study of photochemically reduced colloidal graphene oxide, Colloid Polym. Sci. 292 (2014) 539–546.

[54] J. Ma, J. Liu, W. Zhu, W. Qin, Solubility study on the surfactants functionalized reduced graphene oxide, Colloids Surf A Physicochem Eng Asp 538 (2018) 79–85.

[55] D. Li, M.B. Müller, S. Gilje, R.B. Kaner, G.G. Wallace, Processable aqueous dispersions of graphene nanosheets, Nature Nanotech 3 (2) (2008) 101–105, https://doi.org/10.1038/nnano.2007.451.

[56] Y.-S. Ho, G. McKay, Pseudo-second order model for sorption processes, Process Biochem. 34 (5) (1999) 451–465.

[57] T. Liu, Y. Li, Q. Du, J. Sun, Y. Jiao, G. Yang, Z. Wang, Y. Xia, W. Zhang, K. Wang, H. Zhu, D. Wu, Adsorption of methylene blue from aqueous solution by graphene, Colloids Surf. B Biointerfaces 90 (2012) 197–203, https://doi.org/10.1016/j.colsurfb.2011.10.019.

[58] L. Chen, J. Yang, X. Zeng, L. Zhang, W. Yuan, Adsorption of methylene blue in water by reduced graphene oxide: effect of functional groups, Mater. Express 3 (4) (2013) 281–290.

[59] F. Arias Arias, M. Guevara, T. Tene, P. Angamarca, R. Molina, A. Valarezo, O. Salguero, C. Vacacela Gomez, M. Arias, L.S. Caputi, The adsorption of methylene blue on eco-friendly reduced graphene oxide, Nanomaterials 10 (4) (2020) 681.

[60] A. Molla, Y. Li, B. Mandal, S.G. Kang, S.H. Hur, J.S. Chung, Selective adsorption of organic dyes on graphene oxide: theoretical and experimental analysis, Appl. Surf. Sci. 464 (2019) 170–177, https://doi.org/10.1016/j.apsusc.2018.09.056.

[61] H. Yan, X. Tao, Z. Yang, K. Li, H. Yang, A. Li, R. Cheng, Effects of the oxidation degree of graphene oxide on the adsorption of methylene blue, J. Hazard. Mater. 268 (2014) 191–198, https://doi.org/10.1016/j.jhazmat.2014.01.015.

[62] F.-C. Wu, R.-L. Tseng, S.-C. Huang, R.-S. Juang, Characteristics of pseudo-second-order kinetic model for liquid-phase adsorption: a mini-review, Chem. Eng. J. 151 (1–3) (2009) 1–9.

[63] B. Hameed, A.M. Din, A. Ahmad, Adsorption of methylene blue onto bamboo-based activated carbon: kinetics and equilibrium studies, J. Hazard. Mater. 141 (3) (2007) 819–825.

[64] Sahoo, T. R.; Prelot, B. Adsorption Processes for the Removal of Contaminants from Wastewater: The Perspective Role of Nanomaterials and Nanotechnology. In *Nanomaterials for the detection and removal of wastewater pollutants*; Elsevier, 2020; pp 161–222.

[65] Kumari, P.; Disha; Nayak, M. K.; Dhruwe, D.; Patel, M. K.; Mishra, S. Synthesis and Characterization of Sulfonated Magnetic Graphene-Based Cation Exchangers for the Removal of Methylene Blue from Aqueous Solutions. *Industrial & Engineering Chemistry Research* **2023**, *62* (3), 1245–1256.

[66] E.N. El Qada, S.J. Allen, G.M. Walker, Adsorption of methylene blue onto activated carbon produced from steam activated bituminous coal: a study of equilibrium adsorption isotherm, Chem. Eng. J. 124 (1–3) (2006) 103–110.

[67] N.U.M. Nizam, M.M. Hanafiah, E. Mahmoudi, A.A. Halim, A.W. Mohammad, The removal of anionic and cationic dyes from an aqueous solution using biomass-based activated carbon, Sci. Rep. 11 (1) (2021) 8623, https://doi.org/10.1038/s41598-021-88084-z.

[68] J. Lin, T. Su, J. Chen, T. Xue, S. Yang, P. Guo, H. Lin, H. Wang, Y. Hong, Y. Su, et al., Efficient adsorption removal of anionic dyes by an imidazolium-based mesoporous poly (ionic liquid) including the continuous column adsorption-desorption process, Chemosphere 272 (2021) 129640.

[69] H. Zhang, Y. Li, B. Cheng, C. Ding, Y. Zhang, Synthesis of a starch-based sulfonic ion exchange resin and adsorption of dyestuffs to the resin, Int. J. Biol. Macromol. 161 (2020) 561–572.

[70] S. Zheng, X. Li, X. Zhang, W. Wang, S. Yuan, Effect of inorganic regenerant properties on pharmaceutical adsorption and desorption performance on polymer anion exchange resin, Chemosphere 182 (2017) 325–331.

[71] Tran, M. L.; Van Tran, T. T.; Juang, R.-S.; Nguyen, C. H. Graphene Oxide Crosslinked Chitosan Composites for Enhanced Adsorption of Cationic Dye from Aqueous Solutions. *Journal of the Taiwan Institute of Chemical Engineers* **2023**, *142*, 104678.

[72] Y. Luoyang, H. Wang, W. Yong, J. Li, X. Li, H. Shenghu, N. Ying, Z. Guotao, Blue coke-based activated carbon adsorbents: insights into the efficiency and mechanism of methyl blue removal, Arab. J. Chem. 17 (9) (2024) 105898.

[73] Z. Wu, H. Zhong, X. Yuan, H. Wang, L. Wang, X. Chen, G. Zeng, Y. Wu, Adsorptive removal of methylene blue by rhamnolipid-functionalized graphene oxide from wastewater, Water Res. 67 (2014) 330–344, https://doi.org/10.1016/j.watres.2014.09.026.

[74] E.O. Nwanebu, X. Liu, E. Pajootan, V. Yargeau, S. Omanovic, Electrochemical degradation of methylene blue using a ni-co-oxide anode, Catalysts 11 (2021) 793, https://doi.org/10.3390/catal11070793.

[75] I. Kolthoff, Indicator constants, J. Phys. Chem. 34 (7) (2002) 1466–1483.

[76] S.-L. Hii, S.-Y. Yong, C.-L. Wong, Removal of rhodamine b from aqueous solution by sorption on turbinaria conoides (phaeophyta), J. Appl. Phycol. 21 (2009) 625–631.

[77] I.K. Basha, E.M. Abd El-Monaem, R.E. Khalifa, A.M. Omer, A.S. Eltaweil, Sulfonated graphene oxide impregnated cellulose acetate floated beads for adsorption of methylene blue dye: optimization using response surface methodology, Sci. Rep. 12 (1) (2022) 9339, https://doi.org/10.1038/s41598-022-13105-4.